Francisco Garcia-Moreno[a], Manas Mukherjee[b], Eusebio Solórzano[a], John Banhart[a,b]

[a] Helmholtz-Centre Berlin, Institute of Applied Materials, Berlin, Germany
[b] Technische Universität Berlin, Institute of Materials Science and Technology, Berlin, Germany

Dedicated to Prof. Dr. H.-P. Degischer on occasion of his 65th birthday

Metal foams – towards microcellular materials

Various techniques to manufacture low-density metallic foams containing sub-millimetre or even micrometre-sized pores are discussed and first trial experiments presented. Three strategies are evaluated: use of an intrinsic blowing agent, foaming under high pressure and foam control by mechanical pressure manipulation. In all three cases, average pore diameters well below 1 mm could be achieved for some aluminium or zinc-based foams while keeping the relative density in a range between 20 % and 50 % of the full metal density.

Keywords: Metal foam; Microporous metal; Microcellular metal

1.   Introduction

The mechanical properties of metallic foams are very different to those of dense metals due to the compliance of the structure of foams that consist of an assembly of struts and films. Under high loads such metal foams can be densified at a nearly constant stress level [1]. The collapse process of the foam itself is very complex, characterised by the generation of shear bands in various locations [2]. One reason for the often unpredictable and poorly reproducible behaviour of foams [3] could be their irregular cell structure, the heterogeneous distribution of the metal within the foams and the small number of cells over the cross section of a foamed specimen [4].

The first step to solve the problem associated with the cell structure is to develop methods to characterise it. X-ray radiography and tomography have been successfully used to obtain information on metal foams either ex-situ in various stages of foaming or deformation or even in-situ during foaming or deformation [5]. The imaging methods applied range from very low to very high resolutions depending on which features are of interest. Low-resolution medical scanners have been used to visualise the shear bands in compressed Al foams [2] or to map density fluctuations in a metal foam [6–8]. High-resolution imaging aims more at resolving the details of the cell walls, cracks, internal pores, etc. [9]. Finally X-ray radiography can resolve with high temporal resolution processes inside an emerging metal foam [10–12]. Altogether, those investigations gave hints to why metal foams are so heterogeneous and why this leads to inferior mechanical properties. In the present paper, X-ray radiography and tomography are used to characterise both the foaming process and foam structure respectively.

A strategy to counter the deficiencies mentioned would be to produce foams with much smaller cells and to ensure that these cells are more uniform in size and distribution of the solid material. Unfortunately, under normal atmospheric conditions, 'conventional' aluminium foams rarely exhibit average pore diameters below 3 mm and the distribution is often very broad, especially in foams made by foaming powder compacts [13]. Pore size can be reduced by faster foaming and interrupting before maximum expansion, but this is done at the expense of the achievable porosity level. Increasing ambient pressure has been shown to reduce pores sizes [14,15]. Moreover, very fine porosity has been reported when die casting was applied to fabricate Al and Mg foams under conditions of very fast foaming and cooling

[16]. Finally, replacing the usually used metal hydrides by an intrinsic gas source in the metal powder has also been found to lead to large reductions of cell sizes [17,18].

The goal researchers would like to reach is to make uniform microcellular metallic foams with a low density. Such foams could perform much more efficiently than the present metallic foams. 'Microcellular' would imply pore diameters below 100 µm and high porosities, e.g. above 80 %, which, at the moment, seems too ambitious to achieve by foaming liquid metals but could become viable after further process development.

In order to obtain foams with small pores one has to ensure that many such pores are created in a given volume, i.e. the aspect of nucleation is important. Moreover, one has to prevent pores from merging to bigger ones by coalescence induced by film rupture. Not very much is known about the nucleation of bubbles in metallic foams. Bubble growth can be traced back to their existence in the sub-µm regime [19], but the way they are actually formed is not clear. Film rupture is caused either by film thinning due to liquid removal (drainage) or by destabilising the films mechanically either by overstretching during growth, the action of external stresses or by pressure gradients created by non-uniform gas release from the blowing agent. Sudden temperature changes such as during overheating after contact with hot mould walls or by cooling and solidification can also induce defects and coalescence [20,21]. Possible strategies to counter coalescence include keeping the time in which the foam is liquid as short as possible, avoiding any premature, abrupt and non-controllable gas evolution, e.g. by pre-treating the blowing agent [22], and ensuring a uniform temperature distribution.

In the present paper, the various strategies as shown in Fig. 1 are studied. The starting point is the foaming of 'traditional' powder compacts obtained from metal powder mixtures containing typically 0.5 wt.% TiH_2. Upon heating and melting, these compacts start to expand and form a foam [5]. Replacing the blowing agent by another gas source that releases gas in a more 'gentle' way is believed to lead to much smaller pore sizes (strategy 1). The same applies to high gas pressures applied during foaming (strategy 2) which restrict pore growth. The third strategy employs mechanical pressures to first hinder foam expansion during heating and to control volume, after which the pressure is released to allow for a controlled expansion of the foam, which is so fast that the foam cannot coarsen. A next step would be to combine these strategies. This combination, however, is beyond the scope of the present paper.

2.   Foaming using an intrinsic blowing agent

In order to produce foams with smaller pores, the first strategy is to distribute gas sources more uniformly throughout the sample than known for the usual blowing agent TiH_2. Ideally, the quantity of gas liberated at each source point should be small enough to give rise to the formation of one micropore only. Moreover, coalescence of such pores should be made more difficult. Unfortunately, no known gas source provided by an external chemical or physical blowing agent satisfies this criterion. The most commonly used blowing agents, metal hydrides and carbonates, are far away from being ideal sources due to their non-uniform distribution in the sample and a high specific gas content [23–25].

It is known that the surface of metal powders contains adsorbed gas. If this gas is utilized to produce foams, uniform foam structures can be realised because in this case every metal powder particle and all its surface will release gas and therefore we will have a gas source with a high surface and hence a low area specific gas evolution. This idea has been exploited to manufacture foams from metal powder compacts without addition of any external blowing agent, but by manipulating ambient gas pressure only [26,27], a process which has been named 'pressure induced foaming' or 'PIF'. The total amount of gas adsorbed by metal powders is usually low and therefore yields low expansion values, usually 100–300 % of the original precursor volume. Beside this, the resultant structure is too coarse, with pore diameteres ranging from 3 mm to 5 mm.

Recently it has been observed that pre-alloyed AlMg50 powder contains a considerable amount of hydrogen that is released above 330 °C and shows maximum evolution around 420 °C [28]. This property of AlMg50 powder has been exploited in a recent study where foams were produced from powder compacts containing a few percent of AlMg50 powder [17,18]. Foaming is performed without any pressure manipulating and the AlMg50 powder acts as an *intrinsic* blowing agent here since it acts both as an alloying element and a blowing agent.

Figure 2 shows the foaming behaviour of AlMg15Cu10 and ZnAl3.3Mg3.3 alloys in which the amount of AlMg50 powder is 30 and 6.6 wt.%, respectively. Compared to the use of – usually 0.5 wt.% – TiH_2 as a blowing agent, the volume of the intrinsic blowing agent is one or two orders of magnitude higher. The specific gas content of AlMg50 powder is much smaller than that of TiH_2 powder and therefore gas evolution is comparable in terms of volume but less local and more 'gentle'. This is considered closer to the ideal situation. The melting range of the Al alloy is 450–560 °C, the eutectic temperature of the Zn alloy 340 °C. The Zn alloy expands more than the Al alloy because it begins to melt almost at the onset of gas release from the AlMg50 powder long before the maximum gas release peak. In other words, in the Zn alloy most of the gas is utilised for foaming which is a necessary criterion for an efficient foaming process. In contrast, the Al alloy begins to melt after the gas release peak. As a result, gas losses are more pronounced and hence the expansion is lower. Expansion of the Zn foams increases with increasing foaming temperature, see Fig. 2b. It is also noticeable that the Zn alloy foam is very stable.

Figure 3 shows representative 2D macrostructures of the foams. Aluminium alloy foams contain larger cells (average 1.5 mm) compared to those in Zn alloy foams where the average cell diameter is about 0.7 mm, as determined from the micrographs. The corresponding relative foam densities were 26 %. The Al alloy foams appear almost defect-free with smooth and uniformly curved cell walls. In the Zn alloy foam, some elliptical cells are visible and both small and large cells are present. On the other hand, in the Al alloy foam the cell size distribution is very narrow as visualised in the 3D section obtained by X-ray tomography as shown in Fig. 4. A 3D analysis (Fig. 4b) of the pore size distribution of these foams shows a mono-modal distribution and a mean equivalent pore diameter D_{mean} of about 2 mm. X-ray tomography allows us to verify that the pores in the foam made by following 'strategy 1' are not just much smaller but also very much more equal in size than pores in 'traditional' foams. We have not reached the goal of microporosity yet, but have got much closer considering the starting point of 'conventional' foam.

3. Foaming under elevated gas pressures

A simple but very effective strategy to obtain micropores is to increase the surrounding gas pressure during foaming. According to the ideal gas law, pore volume will decrease in inverse proportion with pressure ($V \sim 1/p$) and therefore pore diameter will scale with $D \sim 1/\sqrt[3]{p}$. Moreover, it is expected that during expansion in high pressure environments there will be less coalescence and hence the final pore structure will be even finer. High pressures are necessary in the heating phase, i.e. during the gas nucleation phase in the precursor, and lead to an increased number of nucleation centres. Pressure manipulation (increase or decrease) after the metal foam has reached a considerable expansion leads to pore volume variation, but also to deformation of pores and deterioration of foam morphology [29]. The reason is the oxidation of the cell walls even from the inner side. Oxidised cell walls corrugate during pressure increase. As a result, the foam volume is decreased but not its surface area.

Following these ideas, foams were produced by heating powder compacts containing Al, Cu and Si powder in fractions that lead to an alloy composition AlSi6Cu4 and some blowing agent TiH_2 and foaming these mixtures in a pressure furnace [30]. The foaming

process was monitored in-situ by X-ray radiography. Automated image analysis software provided the expansion curves shown in Fig. 5a. X-ray tomography was used to visualise the 3D foam structure of the samples after solidification, see Fig. 5b. 3D image analysis was carried out to obtain the 3D pore size distributions and the mean pore diameter shown in Fig. 5c.

The first sample contains 0.5 wt.% of TiH_2 and is foamed under atmospheric pressure. Hence, this is a 'conventional' foam with the difference that heating and therefore expansion are stopped 140 s after the start of heating to keep pores small. This underexpanded sample has a relative density of 38 % and pores with a mean diameter of 0.6 mm. Full expansion of this sample would have led to pore sizes between 3 and 5 mm and the way to prevent this growth was to interrupt foaming early at the cost of achievable foam expansion. The analogous experiment carried out under 40 bar pressure provides a foam with even smaller pores ($D_{mean} = 0.14$ mm), but also a lower expansion and a higher relative density of 57 %. Increasing the amount of blowing agent to 2.5 wt.% and also foaming at 40 bar pressure then leads to a higher expansion – density 46 % – and well distributed small pores ($D_{mean} = 0.16$ mm).

Precursors foamed under increased pressures contain a large amount of both small and round micropores, but mostly show an undesirable high density, as the total gas volume available in the foam is also compressed due to the surrounding overpressure. To compensate for this deficiency in expansion we can increase the amount of blowing agent and therefore the gas volume available. We know from the literature that an increase of the amount of blowing agent does not necessarily lead to higher expansion and therefore to lower density at 1 bar ambient pressure [31]. However, at higher pressures it is found that the blowing agent content that leads to both good expansion and pore structure is much higher, e.g. 2.5 wt.% TiH_2 for AlSi6Cu4 foamed at 40 bar argon [30].

4. Foaming applying mechanical pressure

In contrast to foaming at elevated gas pressure, the methodology applied for 'strategy 3' does not involve the application of any external pressure to the foamable material since the material itself will generate it itself upon heating. The physical principles of this method are similar to those previously described, i.e. high pressure favours the creation of a higher number of nuclei that will increase the final cell density of the foam. To this end, the material needs to be locked in a gas-tight foaming cavity of an initial volume similar to that of the precursor. After the precursor material has melted and the foaming agent is being decomposed, the pressure rises sharply as there is no accessible volume for the foam to expand. This pressure increase is monitored during the process and after melting can reach values up to 450–600 bar. After having held the material for a sufficient time (determined experimentally) above the melting point, the pressure is released by increasing the volume accessible to the molten precursor. This is done by moving a sliding piston, see Fig. 6. The position of this piston is also monitored so that the volume expansion can be controlled. The pressurised foam immediately expands into the new volume. The mould is cooled down immediately after this expansion has completed.

Figure 6 displays a simplified scheme of the set-up used to foam metallic materials by this method. When the piston is closed (a) the movement is locked at nearly zero load by an upper hydraulic press that also allows for monitoring the pressure evolution. In a second moment (b) the piston is unlocked, and the material expands and forms a foam. A displacement control allows for fixing the final expansion ratio $(h-h_0)/h_0$.

One of the main advantages of this method is that foaming can be triggered at any moment after the material has melted at a range of temperatures above the melting point, thus providing precise control over the time and temperature variables. In addition, the expansion step occurs in a very short period – a few seconds – allowing for simultaneous pore growth as

well as reduced coalescence and foam ageing. The reduced time the foam is kept in the liquid state before solidification combined with the initially higher cell densities, contribute to smaller cell sizes at any relative density compared to the standard PM route.

The range of materials produced by this method is restricted to low-melting point alloys such as pure Zn (T_M = 419 ºC) or Zn+6.64 wt.%AlMg50 (T_M = 340 ºC) at the moment because no appropriate mould was available for Al alloys. The alloys were foamed with untreated blowing agents (either TiH_2 or MgH_2). The present temperature restrictions could be overcome by selecting suitable materials for the cavity with sufficient mechanical resistance at the temperatures required to foam, e.g., aluminium alloys.

Average pore sizes below 100 µm and cell densities (number of cells per unit volume) as high as $5 \cdot 10^5$ cells×cm^{-3} have been achieved in the case of dense foams (at about 60 % density). Figure 7 shows the fractured surface of one high density sample produced by this method. A bimodal pore size distribution is observed. In addition, Fig. 8 shows 3D visualisations of samples with different densities (dense and light microporous ZnAlMg). In the case of dense foams (a), it can be observed that the pores are spherical and average cell sizes are below 100 µm, with a high volume fraction of pores below 50 µm. A bimodal pore size distribution seems to be present in this case as well. Figure 8b shows a light foam (density ≈20 %) with a different kind of bimodal of cell size distribution: Here, the majority of the larger pores are around 250 µm in diameter, but it can be observed that a large amount of satellite pores with diameters below 25 µm are dispersed within the cell walls.

5.   Conclusions

All the newly developed foaming methods yielded foams with promising cell size and density parameter combinations. Table 1 summarises the best results. Accordingly, we can make Zn- or Al-based foams with average cell sizes as low as 160 µm while keeping the density at reasonably low levels. Obviously, the final goal of microcellular foams with less than 20 % relative density – or >80 % porosity – has not yet been reached, but a combination of the various methods explored should bring us closer to it.

References

[1] L.J. Gibson, M.F. Ashby: Cellular Solids, Cambridge University Press, Cambridge (1999).
[2] H. Bart-Smith, A.-F. Bastawros, D.R. Mumm, A.G. Evans, D.J. Sypeck, H.N.G. Wadley: Acta Mater. 46 (1998) 3583.
[3] U. Ramamurty, A. Paul: Acta Mater. 52 (2004) 869.
[4] E.W. Andrews, G. Gioux, P. Onck, L.J. Gibson: Int. J. Mech. Sci. 43 (2001) 701.
[5] H.-P. Degischer, B. Kriszt: Handbook of Cellular Metals, Wiley-VCH, Weinheim (2002).
[6] B. Kriszt, B. Foroughi, K. Faure, H.-P. Degischer, in: J. Banhart, M.F. Ashby, N.A. Fleck (Eds.), Metal Foams and Porous Metal Structures, MIT-Verlag, Bremen (1999) 241.
[7] B. Kriszt, B. Foroughi, K. Faure, H.-P. Degischer: Mater. Sci. Technol. 16 (2000) 792.
[8] R. Jancek, A. Kottar H.-P. Degischer, in: J. Banhart, N.A. Fleck, A. Mortensen (Eds.), Cellular Metals – Manufacture, Properties, Applications, MIT-Verlag, Berlin (2003) 19.
[9] A. Elmoutaouakkil, L. Salvo, E. Maire, G. Peix: Adv. Eng. Mater. 4 (2002) 803.
[10] J. Banhart, H. Stanzick, L. Helfen, T. Baumbach, K. Nijhof: Adv. Eng. Mater. 3 (2001) 407.

[11] F. García-Moreno, A. Rack. L. Helfen, T. Baumbach, S. Zabler, N. Babcsán, J. Banhart, T. Martin, C. Ponchut, M. Di Michiel: Appl. Phys. Lett. 92 (2008) 134104.

[12] A. Rack, F. García Moreno, T. Baumbach, J. Banhart: J. Synchrotron Rad. 16 (2009) 432.

[13] D. Leitlmeier, H.-P. Degischer, H. Flankl: Adv. Eng. Mater. 4 (2002) 735.

[14] C. Körner, F. Berger, M. Arnold, C. Stadelmann, R.F. Singer: Mater. Sci. Technol. 16 (2000) 781.

[15] F. Simancik, N. Minarikova, S. Culak, J. Kovacik, in: J. Banhart, M.F. Ashby, N.A. Fleck (Eds.), Metal Foams and Porous Metal Structures, MIT Publishing, Bremen (1999) 105.

[16] C. Körner: Integral Foam Molding of Light Metals, Springer, Berlin, Heidelberg (2008).

[17] M. Mukherjee, C. Jimenez, F. Garcia-Moreno, J. Banhart: German Patent Application DE 10 2009 020 004.5, 2009.

[18] M. Mukherjee, F. Garcia-Moreno, C. Jimenez, J. Banhart: Adv. Eng. Mater. (in print, 2010), doi: 10.1002/adem.201000017.

[19] J. Banhart, D. Bellmann, H. Clemens: Acta Mater. 49 (2001) 3409.

[20] H. Stanzick, M. Wichmann, J. Weise, L. Helfen, T. Baumbach, J. Banhart: Adv. Eng. Mater. 4 (2002) 814.

[21] M. Mukherjee, F. Garcia Moreno, J. Banhart: Scripta Mater. 63 (2010) 235.

[22] B. Matijasevic, J. Banhart: Scripta Mater. 54 (2006) 503.

[23] F. von Zeppelin, M. Hirscher, H. Stanzick, J. Banhart: Comp. Sci. Technol. 63 (2003) 2293.

[24] D. Lehmhus, G. Rausch: Adv. Eng. Mater. 6 (2004) 313.

[25] B. Matijasevic, J. Banhart, S. Fiechter, O. Görke, N. Wanderka: Acta Mater. 54 (2006) 1884.

[26] F. Garcia-Moreno, J. Banhart: German Patent DE 10 2005 037 305 B4 (2005).

[27] F. Garcia-Moreno, J. Banhart: Coll. Surf. A 309 (2007) 264.

[28] C. Jimenez, F. Garcia-Moreno, J. Banhart, G. Zehl, in: L.P. Lefebvre, J. Banhart, D. Dunand (Eds), Porous Metals and Metallic Foams, DEStech Publications, Pennsylvania (2008) 59.

[29] F. García-Moreno, N. Babcsan, J. Banhart: Coll. Surf. A 263 (2005) 290.

[30] F. Garcia-Moreno et al.: unpublished results.

[31] H. Stanzick, I. Duarte, J. Banhart: Materialwiss. u. Werkstofftech. 31 (2000) 409.

Table 1. Selected results for foams produced by one of the strategies tested in the present work.

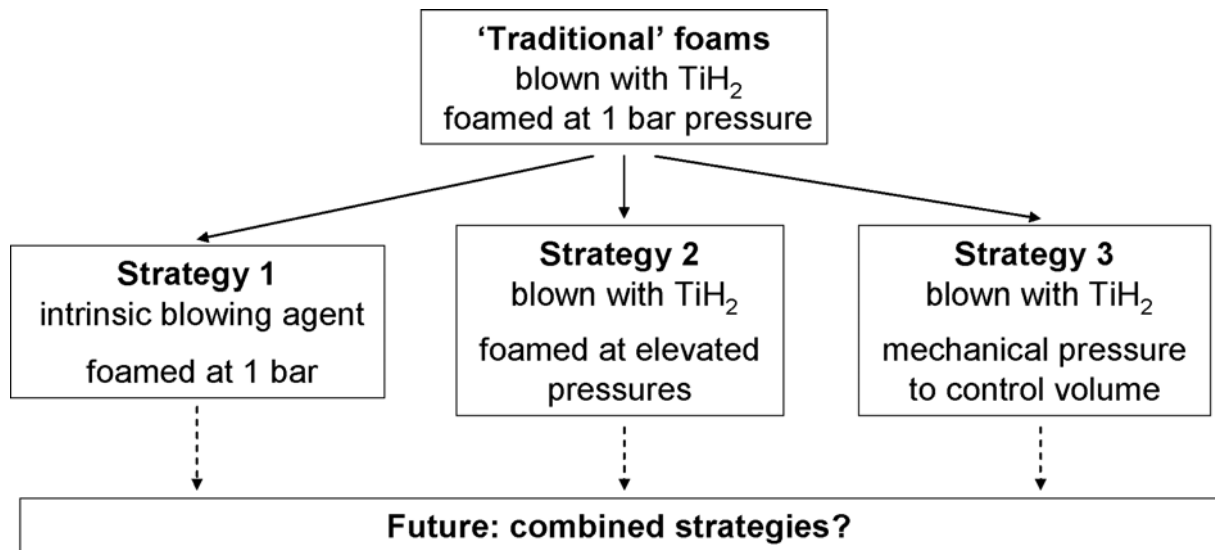|	alloy	relative density (%)	average pore size (μm)	image
1. intrinsic gas source	Zn-based	26	700	Fig. 3b
2. gas pressure	Al-based	46	160	Fig. 5b
3. mechanical volume control	Zn-based	20	250	Fig. 8b

Figure 1: Some strategies for the development of microcellular metal foam.

(a)

(b)

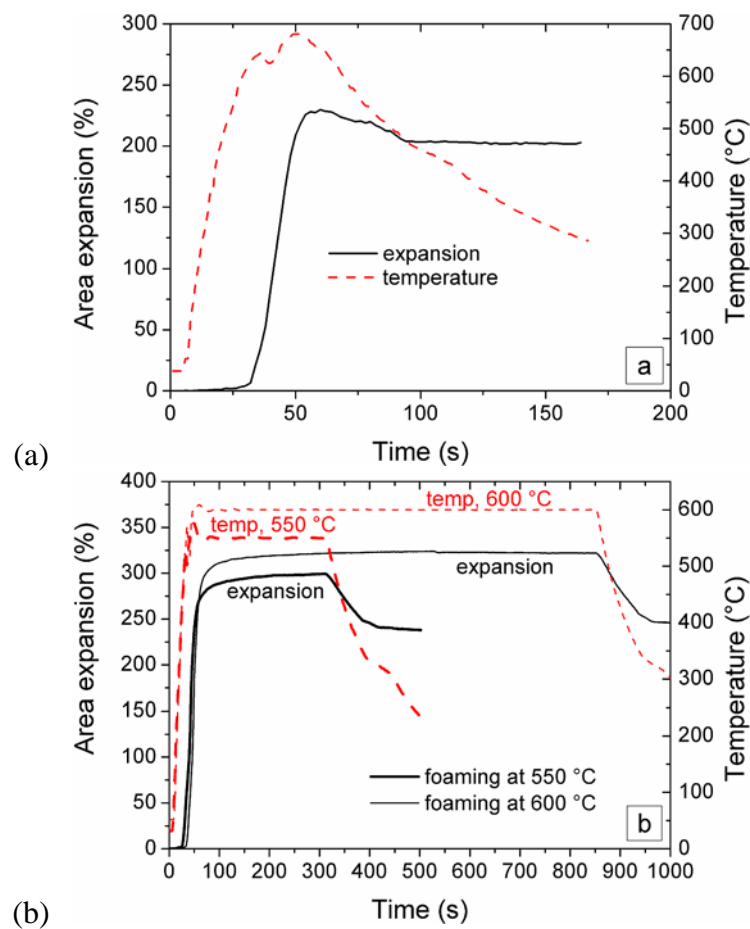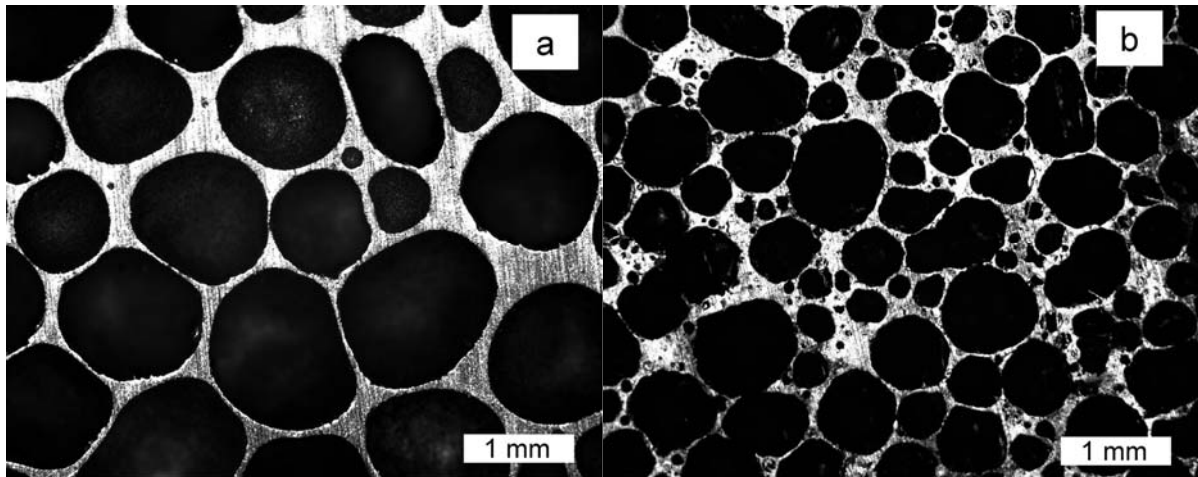Figure 2: Expansion behaviour of (a) AlMg15Cu10 and (b) ZnAl3.3Mg3.3 alloys

Figure 3: Pore structure of (a) AlMg15Cu10 and (b) ZnAl3.3Mg3.3 foam

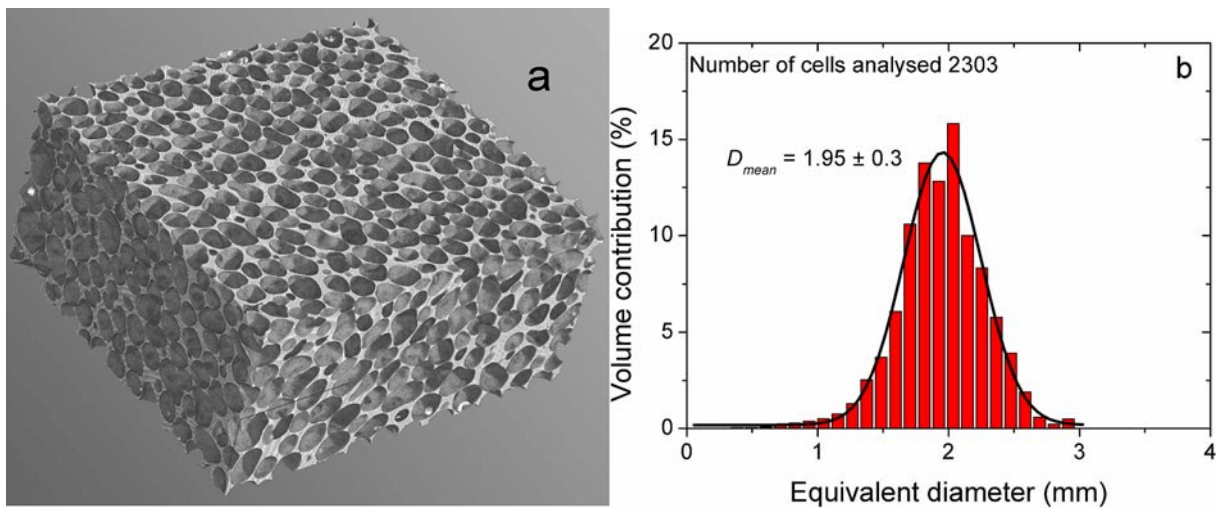
Figure 4: (a) 3D visualisation of X-ray tomographic reconstruction of AlMg15Cu10 foam, Dimension: $20 \times 20 \times 10$ mm^3. (b) Corresponding 3D pore size distribution fitted with a Gaussian distribution curve (reported in Ref. 18).
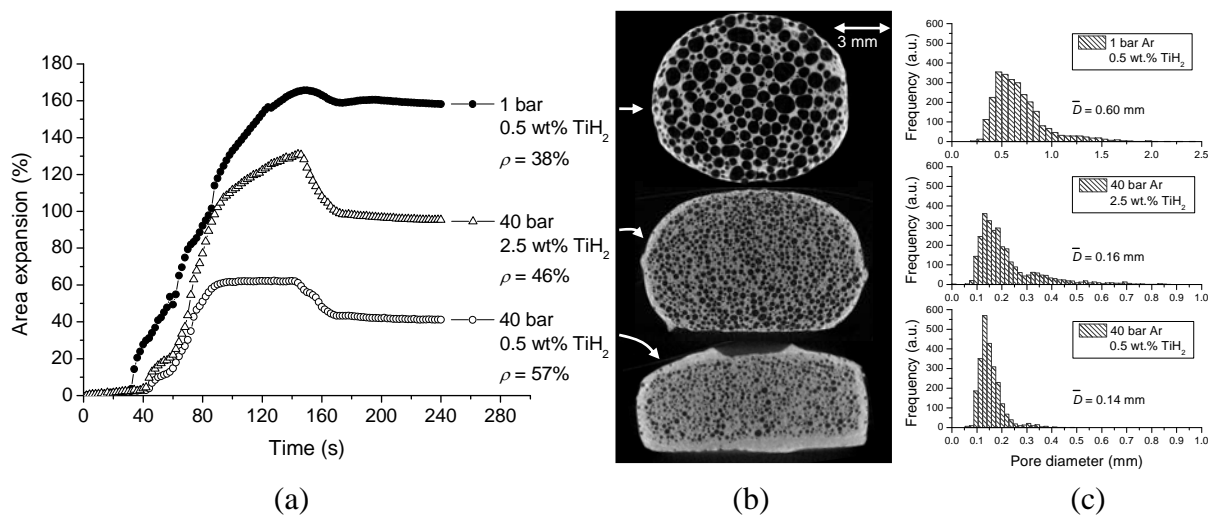
Figure 5: (a) Area expansion during foaming, (b) pore structure and (c) 3D pore size distribution of AlSi6Cu4 foams foamed with 1 and 2.5 wt.% TiH_2 under 1 or 40 bar argon pressure.
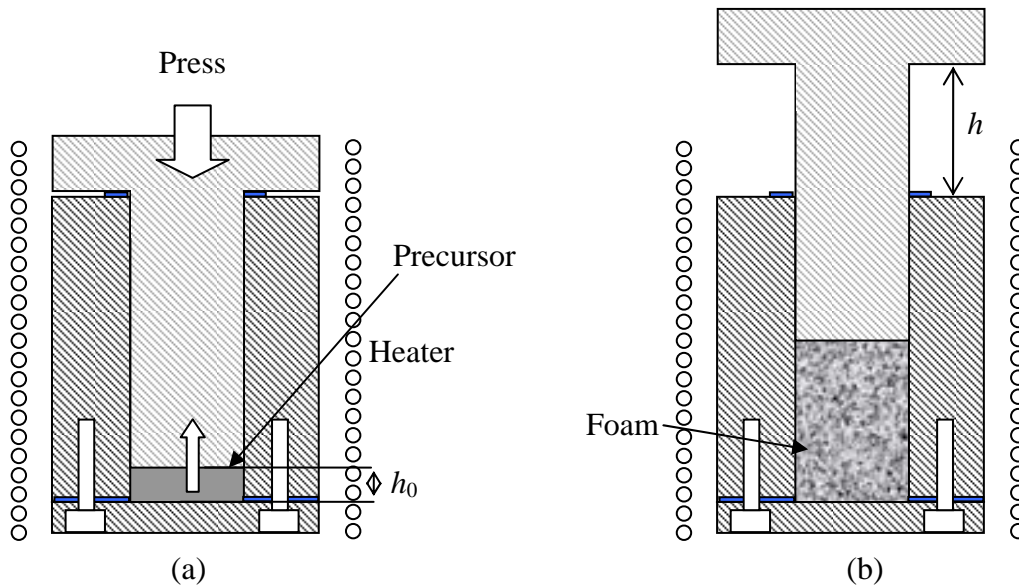

Figure 6. Simplified sketch of two stages of the foaming process, (a) before and (b) after foam expansion.
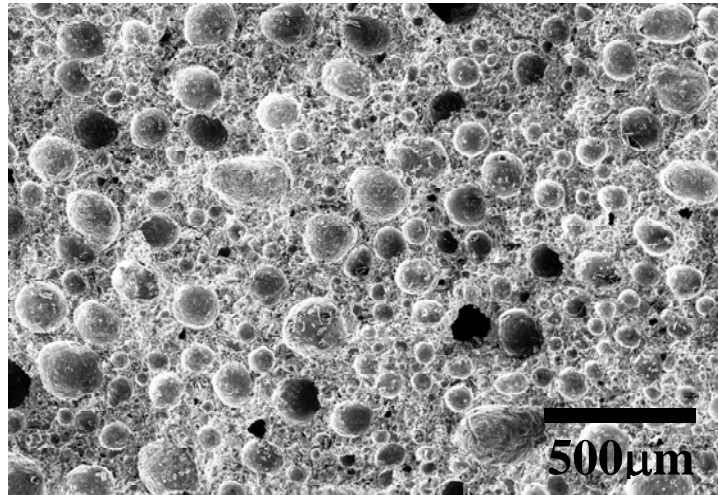
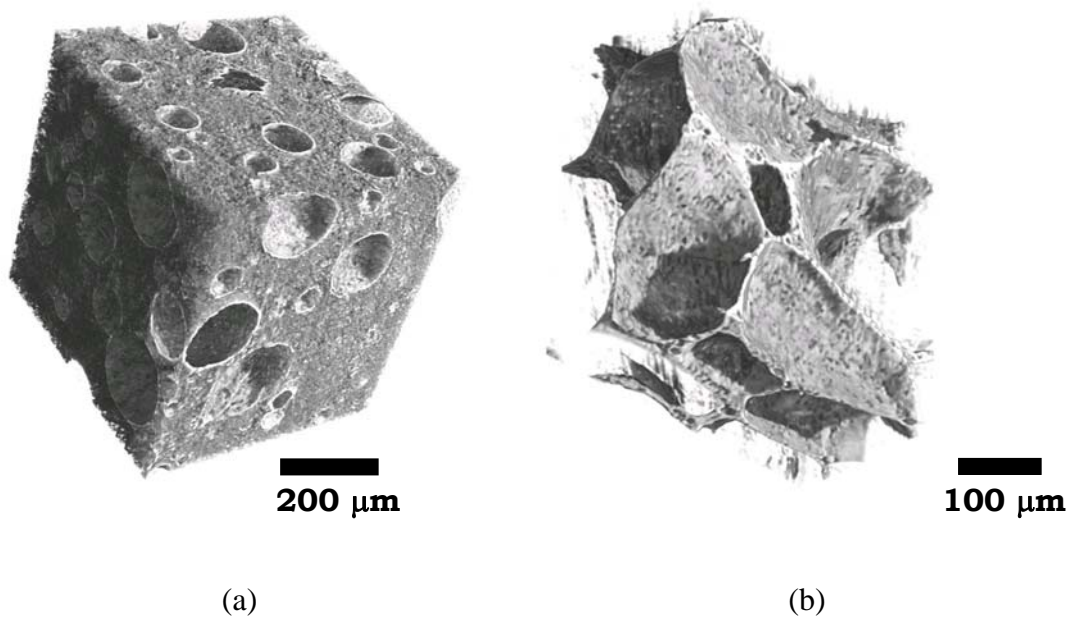Figure 7. SEM micrograph of a ZnAlMg foam with a relative density ≈60 %.

(a)   (b)

Figure 8. 3D rendering of synchrotron X-ray microtomographies of ZnAlMg foams:
(a) ≈60 % density (b) ≈20 % density.